Journal of Power Sources 196 (2011) 1036–1041

Contents lists available at ScienceDirect

Journal of Power Sources

journal homepage: www.elsevier.com/locate/jpowsour

Ethane dehydrogenation over nano-Cr_2O_3 anode catalyst in proton ceramic fuel cell reactors to co-produce ethylene and electricity

Xian-Zhu Fu[a], Xiao-Xiong Luo[a], Jing-Li Luo[a,*], Karl T. Chuang[a], Alan R. Sanger[a], Andrzej Krzywicki[b]

[a] Department of Chemical and Materials Engineering, University of Alberta, Edmonton, Alberta T6G2G6, Canada
[b] NOVA Chemicals Corp., Calgary, Alberta T2P5C6, Canada

ARTICLE INFO

Article history:
Received 25 June 2010
Received in revised form 6 August 2010
Accepted 9 August 2010
Available online 21 August 2010

Keywords:
Anode catalyst
Ethane dehydrogenation
Doped barium cerate proton conductor
Solid oxide fuel cells
Carbon deposition

ABSTRACT

Ethane and electrical power are co-generated in proton ceramic fuel cell reactors having Cr_2O_3 nanoparticles as anode catalyst, $BaCe_{0.8}Y_{0.15}Nd_{0.05}O_{3-\delta}$ (BCYN) perovskite oxide as proton conducting ceramic electrolyte, and Pt as cathode catalyst. Cr_2O_3 nanoparticles are synthesized by a combustion method. $BaCe_{0.8}Y_{0.15}Nd_{0.05}O_{3-\delta}$ (BCYN) perovskite oxides are obtained using a solid state reaction. The power density increases from 51 mW cm^{-2} to 118 mW cm^{-2} and the ethylene yield increases from about 8% to 31% when the operating temperature of the solid oxide fuel cell reactor increases from 650 °C to 750 °C. The fuel cell reactor and process are stable at 700 °C for at least 48 h. Cr_2O_3 anode catalyst exhibits much better coke resistance than Pt and Ni catalysts in ethane fuel atmosphere at 700 °C.

1. Introduction

Ethane is present at levels up to several percent in many natural gas deposits, and is also formed as a by-product of petroleum refining. Its main use is as petrochemical feedstock to produce ethylene, a major intermediate in manufacture of polymers and petrochemicals [1]. Its potential has been recognized as a fuel for hydrocarbon solid oxide fuel cells to generate electrical energy with high efficiency and low impact on the environment, in which it is oxidized deeply to CO_2 and H_2O [2–5]. To more efficiently utilize ethane resources, ethane proton ceramic fuel cell reactors have been developed having several specific advantages including [6–9]: (1) value-added ethylene can be co-generated with power; (2) there are no greenhouse gas (CO_2) emissions, in contrast to oxygen ion solid oxide fuel cells; (3) ethylene can be obtained with higher selectivity and no detectable amounts of acetylene, in contrast to conventional steam cracking processes.

In a proton conducting fuel cell reactor, ethane is dehydrogenated to ethylene over the anode catalyst, protons are conducted through the proton conducting electrolyte to form water by reacting with oxygen at the cathode, and electrons are conducted through an external circuit. Although several proton conductors and cathode materials have been reported for proton conducting solid oxide fuel cells [10–22], there are very few practical anode catalysts identified for hydrocarbon proton conducting solid oxide fuel cells [5]. In our previous study, we used Pt as anode catalyst for ethane solid oxide fuel cells due to its high ethane dehydrogenation activity; however Pt is expensive and easily poisoned by carbon deposition at fuel cell operating temperatures [7,8]. Consequently we have investigated alternative anode materials for selective conversion of hydrocarbons. Herein we describe use of Cr_2O_3 nanoparticles as anode catalysts for ethane dehydrogenation in high performance proton ceramic fuel cell reactors for co-producing ethylene and electrical power.

2. Experimental

2.1. Materials preparation and characterization

Cr_2O_3 nanopowders were prepared by a combustion method. $Cr(NO_3)_3{\cdot}6H_2O$ salt was first dissolved in deionized water. Subsequently, citric acid as chelating agent was added in 2:1 molar ratio to Cr ions. The resulting solution was adjusted to about pH 8 with ammonia hydroxide then heated on a hot plate to evaporate water at 90 °C until it formed a gel which was then dried. The dry gel was calcined at 500 °C for 2 h, the temperature shown to be suitable using TA SDT Q600 thermal gravity analysis (TGA) of dry gel in air. Temperature programmed oxidation (TPO) analysis was performed using TGA combined with a Pfeiffer Thermostar GSD 301 mass spectrometer (MS). Samples for TGA-DSC–MS tests were

* Corresponding author. Tel.: +1 780 492 2232; fax: +1 780 492 2881.
E-mail address: Jingli.Luo@ualberta.ca (J.-L. Luo).

0378-7753/$ – see front matter © 2010 Elsevier B.V. All rights reserved.
doi:10.1016/j.jpowsour.2010.08.043

5 mg, the flow gas of air was 100 mL min^{-1}, and the heating rate was 10 °C min^{-1}.

$BaCe_{0.8}Y_{0.15}Nd_{0.05}O_{3-\delta}$ (BCYN) perovskite powders were synthesized using a solid state reaction from stoichiometric amounts of $BaCO_3$, CeO_2, Y_2O_3 and Nd_2O_3. Mixtures were ball-milled for 24 h, and then calcined at 1300 °C for 10 h in air. The resulting materials were ball-milled again for 24 h, pressed at 5 tons into discs with a diameter of 1.86 cm and a thickness about 2 mm, and sintered at 1500 °C for 10 h in air to obtain high-density membranes. After sintering, the BCYN discs were polished and reduced to 1 mm thickness.

Platinum paste was applied on one side of the polished discs and dried to form 0.5 cm^2 electrodes, then heated at 900 °C for 30 min. An intimate mixture of 40% Cr_2O_3 and 60% Cu powders then was dispersed in terpineol mixed with 10% polyethylene glycol (PEG) as screen printing binder to form a paste which was screen painted onto the opposite face of the electrolyte and dried under infrared light to form 0.5 cm^2 anodes. Cr_2O_3 served as anode catalyst and Cu improved electrical conductivity of the anode.

The phase structures of materials were identified using a Rigaku Rotaflex X-ray diffractometer (XRD) with Co Kα radiation. The shapes and particle sizes of powders were determined using a Philips Morgagni 268 transmission electron microscope (TEM). Morphology of sintered BCYN disc cross-section was determined using a Hitachi S-2700 scanning electron microscope (SEM). X-ray photoelectron spectroscopy (XPS) was performed in a Kratos Analytical AXIS 165. A monochromated Al Kα ($h\nu$ = 1486.6 eV) source was used at a power of 210 W, with a base pressure of 3×10^{-8} Pa in the analytical chamber. The spectra were referenced to C 1s biding energy of 284.6 eV and fitted using Gaussian–Lorentzian peak shapes and Shirley baselines.

2.2. Fuel cell reactor system fabrication and testing

The fuel cell reactor was set up by securing the MEA (membrane electrode assembly) between coaxial pairs of alumina tubes and sealed using ceramic sealant, which was cured by heating in a vertical Thermolyne F79300 tubular furnace. Au paste and mesh were used as current collector at the anode. 10% H_2 (balance with He) was fed into the anode chamber as the temperature was increased from room temperature to 750 °C at 1 °C min^{-1}. Then, ethane was fed into the anode chamber to replace 10% H_2 gas. Oxygen was the cathode feed.

The conductivity of BCYN perovskite electrolyte and the electrochemical performance of fuel cell reactor were measured using a Solartron 1287 electrochemical interface together with 1255B frequency response analysis instrumentation. The outlet gases from the anode chamber were analyzed using a Hewlett-Packard model HP5890 GC equipped with a packed bed column (OD: 1/8 IN.; length: 2 m; Porapak QS) operated at 80 °C and equipped with a thermal conductivity detector. The fuel cell reactor set-up and test system are shown schematically in Fig. 1. The ethane conversion, ethylene selectivity and yield were calculated according to the previously reported method and defined as [6]:

$$C_2H_6 \text{ conversion} = \left[\frac{\text{moles of } C_2H_6 \text{ converted}}{\text{moles of } C_2H_6 \text{ introduced}}\right] \times 100\% \quad (1)$$

$$C_2H_4 \text{ selectivity} = \left[\frac{\text{moles of } C_2H_4 \text{ produced}}{\text{moles of } C_2H_6 \text{ converted}}\right] \times 100\% \quad (2)$$

$$C_2H_4 \text{ yield} = \left[\frac{\text{moles of } C_2H_4 \text{ converted}}{\text{moles of } C_2H_6 \text{ introduced}}\right] \times 100\% \quad (3)$$

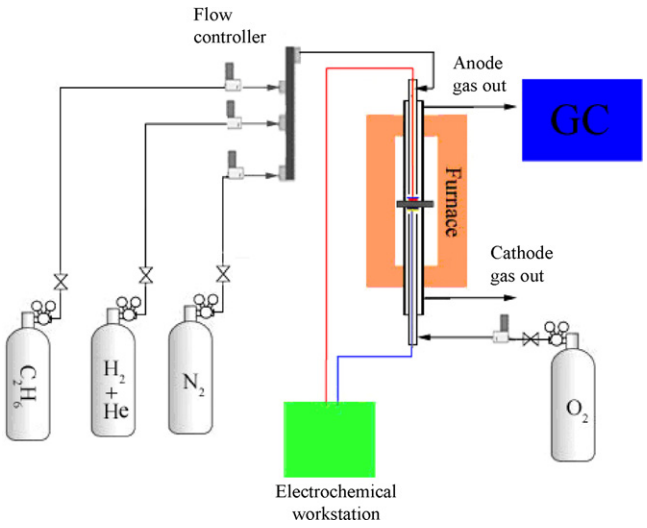

Fig. 1. Schematic of proton ceramic fuel cell reactor set-up and test system.

3. Results and discussion

3.1. Thermal analysis of Cr–citrate complex

The thermal decomposition procedure of the Cr–citrate complex gel was monitored using TGA-DSC analysis (Fig. 2). There was continuous weight loss totalling about 90% as the sample was heated from room temperature to 500 °C. The slow weight loss of ~2% below ~130 °C was attributed primarily to evaporation of water. The rapid weight loss of ~40% in the range 130–300 °C was attributed to the decomposition of a portion of the organic matter in the citrate complex. There was a dramatic weight loss of ~48% and corresponding heat flow peak greater than 18 W g^{-1} between ~300 °C and ~400 °C, resulting from the combustion of NH_4–NO_3 and oxidation of any residual organic matter. There was no obvious further weight loss above 500 °C, which suggested that the Cr–citrate gel was completely decomposed to oxides below 500 °C in air. Consequently, the dry gel was heated to 500 °C to prepare Cr_2O_3 powders.

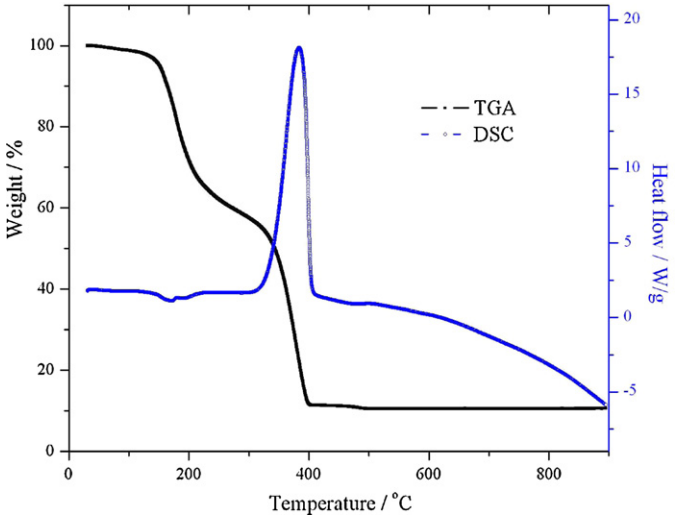

Fig. 2. TGA-DSC curves of Cr–citrate–nitrate gel.

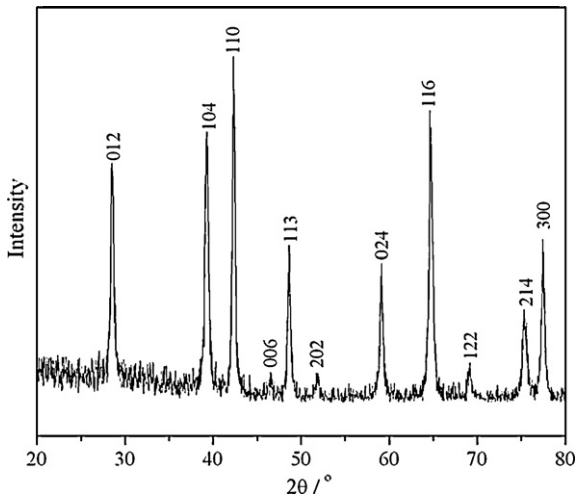

Fig. 3. XRD pattern of as-prepared Cr_2O_3 powder.

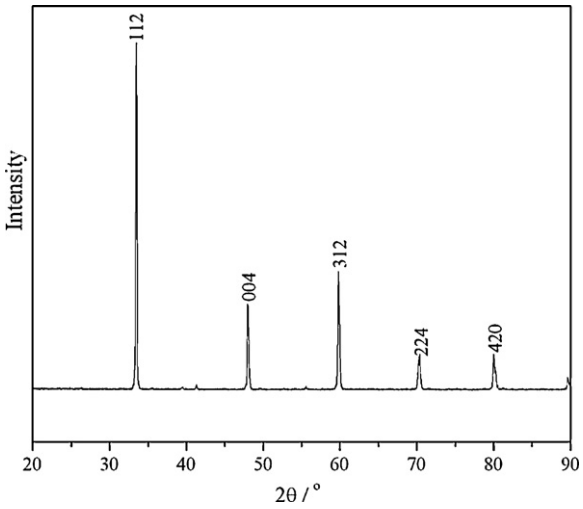

Fig. 5. XRD pattern of as-prepared BCYN perovskite oxide.

3.2. Characterization of as-prepared Cr_2O_3 powders

XRD (Fig. 3) confirmed that Cr_2O_3 was formed after calcination of the Cr–citrate complex gel at 500 °C for 2 h in air. The Cr_2O_3 formed using this process consisted of very fine particles, mainly smaller than 20 nm (TEM, Fig. 4). Hence use of citrate as a chelating agent provided good distribution of Cr ions in the dry gel, and the process generated large amounts of gas during the citrate–nitrate gel combustion and decomposition, resulting in formation of very fine Cr_2O_3 particles.

3.3. Structure and conductivity of BCYN electrolyte

BCYN prepared via solid state reaction was a pure perovskite oxide (XRD, Fig. 5). Cross-sectional SEM image (Fig. 6) showed that BCYN membranes sintered at 1500 °C were very dense. The conductivity of BCYN perovskite electrolyte increased from 25.7 mS cm^{-1} to 52.9 mS cm^{-1} when the fuel cell reactor operating temperature increased from 650 °C to 800 °C (Fig. 7), which was higher conductivity than that of BCY used in our previous study under ethane fuel cell operating conditions [7]. Thus, as found previously for BCYN prepared by the Pechini method [23], doping of Nd into BCY

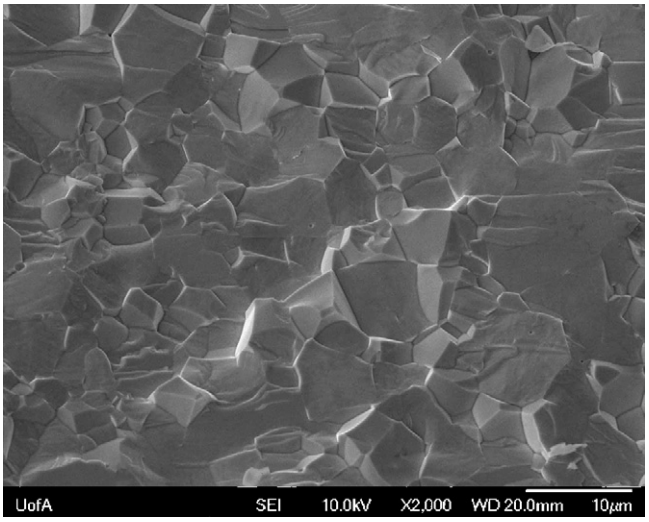

Fig. 6. Cross-sectional SEM image of BCYN ceramic electrolyte membrane.

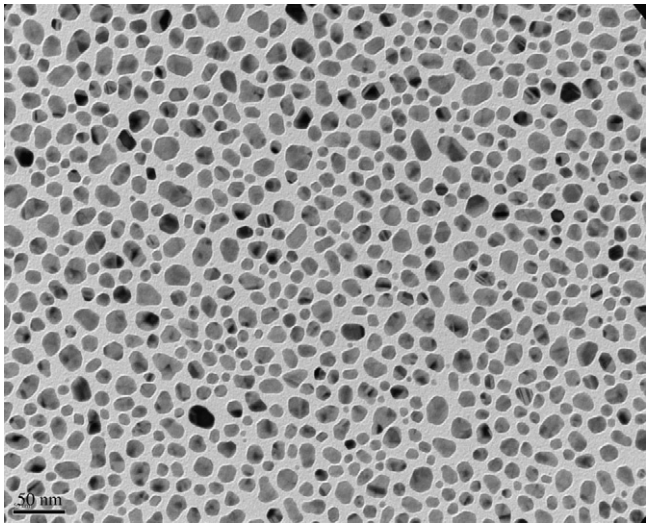

Fig. 4. TEM image of as-prepared Cr_2O_3 powder.

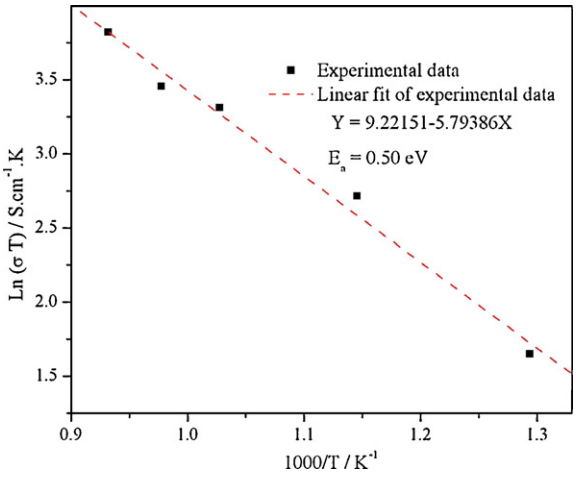

Fig. 7. Conductivity of BCYN electrolyte under proton ceramic fuel cell reactor conditions. The flow rates of ethane and oxygen each are 150 mL min^{-1}.

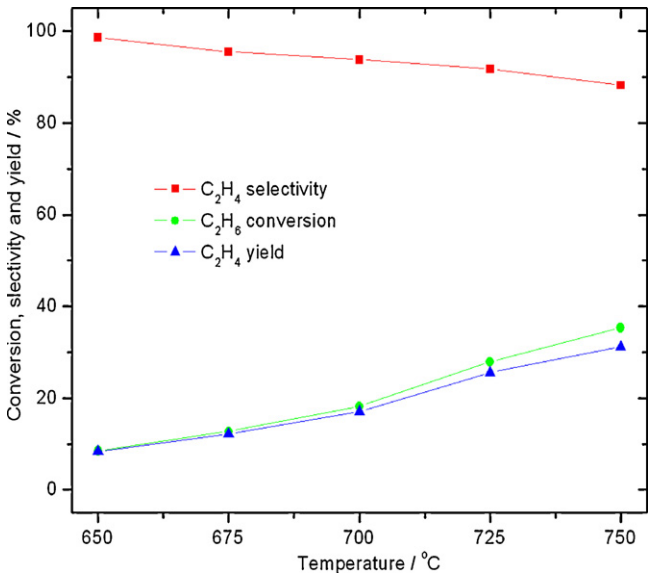

Fig. 8. Ethane conversion, ethylene selectivity and yield in proton ceramic fuel cell reactor under open-circuit conditions. The flow rates of ethane and oxygen each are 150 mL min^{-1}.

perovskite oxide using the present method also improved its conductivity.

3.4. Ethane dehydrogenation over Cr_2O_3 anode catalyst

The main reaction in the anode chamber is dehydrogenation of ethane to ethylene with high selectivity, arising from several factors. Cr_2O_3 is an excellent dehydrogenation catalyst, and so dehydrogenation of ethane to ethylene occurred readily [24]. The proton conducting ceramic electrolyte membrane prevented contact with any oxygen source. The proton ceramic electrolyte membrane conducted the protons to the cathode to react with oxygen and form water, thus providing the thermodynamic driving force and removing equilibrium limitation of the dehydration reaction. Conversion of ethane increased from 8.5% to 35.3% whilst the selectivity of ethylene decreased from 98.6% to 88.2% (Fig. 8), so the ethylene yield increased from 8% to 31% as the operating temperature increased from 650 to 750 °C. However, as the rate of dehydrogenation of ethane to ethylene increased with temperature, by-product formation also became faster. GC analysis showed that there were also small amounts of methane and hydrogen, and traces of carbon oxides, in addition to ethane and ethylene in the outlet stream from the anode compartment fed with dry ethane.

The hydrogen in the anode outlet was attributable to either or both of gas phase cracking of ethane to ethylene and combination of the accommodated protons which were produced from the cleavage of C–H bond as ethane dehydrogenated over Cr_2O_3 anode catalyst but did not transported through the thick electrolyte membrane in time. Methane was produced from the thermal cracking of ethane which was more favoured at the higher temperature, so that ethylene selectivity decreased while methane selectivity increased at the higher operating temperature. The source of the trace amounts of carbon oxides was not clear. Possibilities included oxidation of ethane by oxygen from a very small oxide ion current through the doped barium cerate electrolyte, counter to the proton current, at high temperature, or diffusion of undetected small amounts of oxygen which diffused into the anode chamber through the fuel cell sealant [25,26]. Fig. 9 showed the $Cr2p_{3/2}$ XPS spectra over Cr_2O_3 anode catalyst before and after test. The binding energy (BE) of $Cr2p_{3/2}$ signals at about 576, 577, and 579 eV was attributed to Cr^{2+}, Cr^{3+}, and Cr^{6+} species, respectively [27,28]. The surface

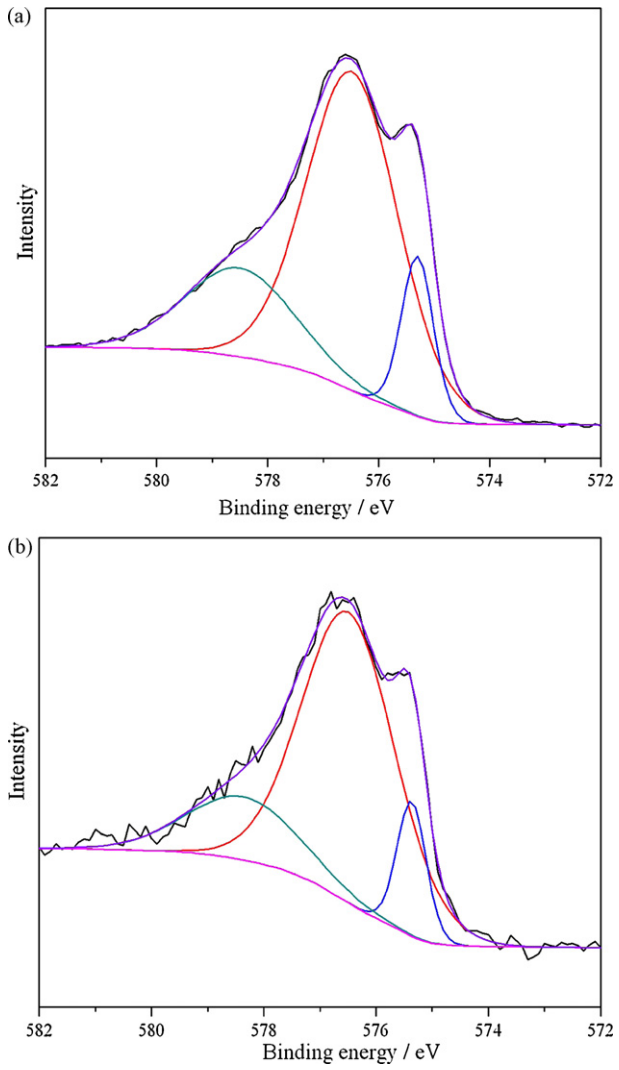

Fig. 9. XPS spectra of $Cr2p_{3/2}$ over Cr_2O_3 anode catalysts before (a) and (b) after test.

concentration of Cr species was given in Table 1. The results displayed that the concentration of Cr^{2+} species had no obvious change while the concentration of Cr^{3+} species increased and the concentration of Cr^{6+} species decreased after test. Therefore, the carbon oxides also might be from the oxidation of ethane by Cr_2O_3 anode catalyst.

Conversion of ethane increased with discharging current density as a function of temperature (Fig. 10), because removal of protons from the anode was more rapid at larger discharging current density. Ethane conversion also increased with temperature when the discharging current density was held constant, showing that the electrochemical dehydrogenation reaction was enhanced at higher temperature. Thus ethane conversion increased with both temperature, hence the enhanced dehydrogenation reaction rate, and ion current density.

Table 1
Cr surface concentration of the Cr_2O_3 anode catalyst before and after test.

	As-prepared Cr_2O_3		Cr_2O_3 after test	
	BE(eV)	Concentration	BE(eV)	Concentration
Cr^{2+}	575.3	11.6%	575.4	11.3%
Cr^{3+}	576.5	66.5%	576.5	71.1%
Cr^{6+}	578.5	21.9%	578.4	17.6%

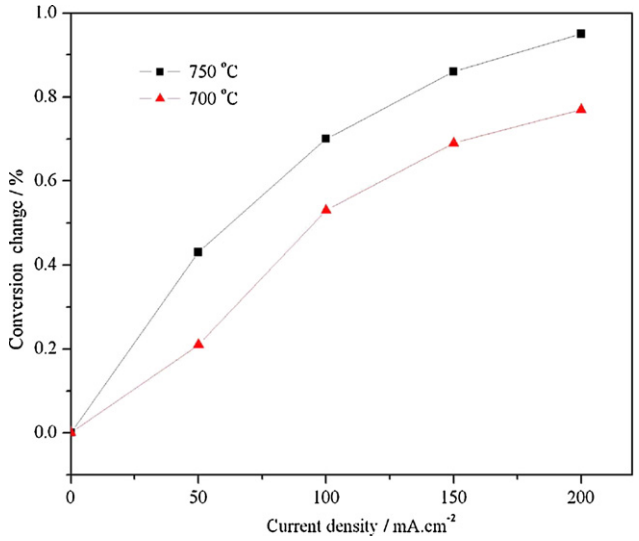

Fig. 10. Change of ethane conversion at different current densities in proton ceramic fuel cell reactors. The flow rates of ethane and oxygen each are 150 mL min^{-1}.

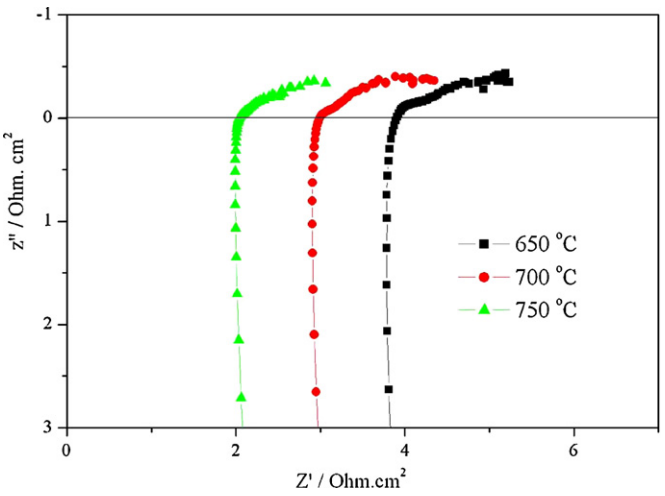

Fig. 12. Electrochemical impedance spectra (EIS) of proton ceramic fuel cell reactors. The flow rates of ethane and oxygen each are 150 mL min^{-1}.

3.5. Electrochemical performance of proton ceramic fuel cell reactors

During ethane dehydrogenation over Cr_2O_3 anode catalyst, electrons were conducted to the outer circuit through the Cu electrical conductor within the anode, and protons were conducted to the cathode via the electrolyte, thereby generating electrical energy. The voltage–current and power density curves of the fuel cells are presented in Fig. 11. At 650 °C, the maximum power density of the fuel cell was 51 mW cm^{-2} at current density 95 mA cm^{-2}. The maximum power density increased with reactor temperature. At 750 °C, the maximum power density was 118 mW cm^{-2} at current density 230 mA cm^{-2}. Both of the rates of dehydrogenation of ethane over the anode catalyst and proton conductivity of BCYN electrolyte were enhanced at higher temperature, resulting in higher power density. The performance of the fuel cell with Cr_2O_3 anode catalyst was comparable to that with Pt anode catalyst [6]. Furthermore, Cr_2O_3 is much lower in cost than Pt, and so offers economic benefit for use as fuel cell catalyst. Fig. 12 shows the electrochemical impedance spectra (EIS) of the ethane fuel cell under open-circuit conditions. The intercepts with the real axis at high frequency and the succeeding semi-circle were assigned to electrolyte ohmic and electrode polarization resistances, respectively. Both the ohmic resistance of the electrolyte and electrode polarization of fuel cell decreased when the operating temperature increased, consistent with results of fuel cell power tests.

The power density of the fuel cell at 700 °C showed no apparent change during 48 h operation (Fig. 13), which indicated that the ethane fuel cell had good stability. The stability was attributed, at least in part, to both Cr_2O_3 catalyst and Cu electron conductor having low carbon deposition activity, and to chemical and physical stability of the electrolyte under the operating conditions. To compare the carbon deposition on anode catalysts, the Cr_2O_3, Pt and Ni powders were treated in ethane at 700 °C for 10 h then heated in air with TPO technique. Fig. 14 illustrated that there was almost no CO_2 emission when the treated Cr_2O_3 was heated in the air comparing to the large peaks of CO_2 signal intensity of Ni and Pt catalysts. The results suggested that Cr_2O_3 anode material had much better coke resistance than Pt and Ni anode catalysts in ethane fuel at 700 °C. Thus, in addition to its low cost, use of Cr_2O_3 as anode catalyst has technical advantages over Pt and Ni, which readily resulted in coking in dry ethane fuel at 700 °C.

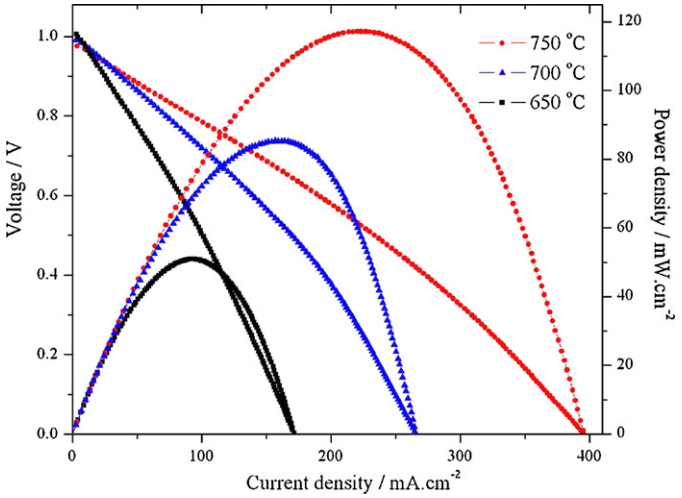

Fig. 11. Current density–voltage and power density curves of proton ceramic fuel cell reactor. The flow rates of ethane and oxygen each are 150 mL min^{-1}.

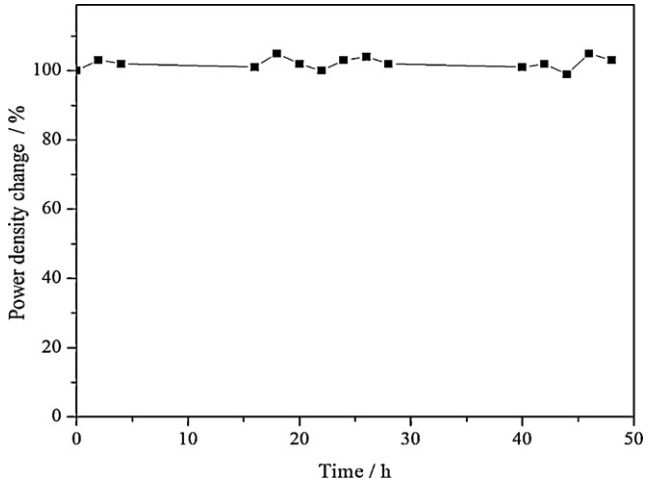

Fig. 13. Power density change of proton ceramic fuel cell reactors at 700 °C with time on stream. The flow rates of ethane and oxygen each are 150 mL min^{-1}.

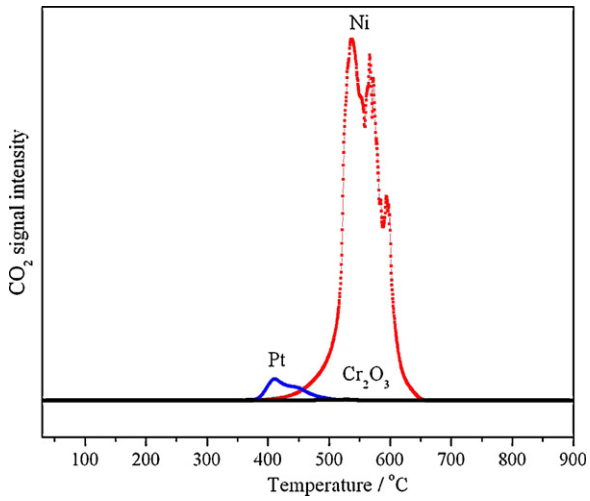

Fig. 14. O_2-TPO curves of Pt and Cr_2O_3 anode catalysts after treatment in dry ethane at 700 °C for 10 h.

4. Conclusion

Cr_2O_3 nanoparticles prepared by a sol–gel combustion method are effective and stable anode catalysts for ethane dehydrogenation to ethylene in solid oxide fuel cell reactors using $BaCe_{0.8}Y_{0.15}Nd_{0.05}O_{3-\delta}$ (BCYN) as proton conducting ceramic electrolyte. The BCYN electrolyte has higher conductivity than $BaCe_{0.85}Y_{0.15}O_{3-\delta}$ (BCY) under the ethane fuel cell operating conditions. The solid oxide fuel cell reactor exhibits high selectivity for ethane dehydrogenation to ethylene yield: 8.3, 17.1 and 31.1%, co-generating 51, 85, and 118 mW cm^{-2} at 650, 700, and 750 °C, respectively. Operation of the fuel cell was stable over 48 h at 700 °C.

Acknowledgements

This work was supported by Natural Sciences and Engineering Research Council of Canada/NOVA Chemicals CRD Grant, the COURSE program of Alberta Innovates Energy and Environment Solutions and Micro Systems Technology Research Institute. The authors also thank Dr. Juri Melnik for very helpful discussions.

References

[1] A.S. Bodke, D.A. Olschki, L.D. Schmidt, E. Ranzi, Science 285 (1999) 712–715.
[2] T. Hibino, A. Hashimoto, T. Inoue, J. Tokuno, S. Yoshida, M. Sano, Science 288 (2000) 2031–2033.
[3] S.D. Park, J.M. Vohs, R.J. Gorte, Nature 404 (2000) 265–266.
[4] D. Hirabayashi, A. Tomita, M.E. Brito, T. Hibino, U. Harada, M. Nagao, M. Sano, Solid State Ionics 168 (2004) 23–29.
[5] A. Tomita, K. Tsunekawa, T. Hibino, S. Teranishi, Y. Tachi, M. Sano, Solid State Ionics 177 (2006) 2951–2956.
[6] S.Y. Wang, J.L. Luo, A.R. Sanger, K.T. Chuang, J. Phys. Chem. C 111 (2007) 5069–5074.
[7] Z.C. Shi, J.L. Luo, S.Y. Wang, A.R. Sanger, K.T. Chuang, J. Power Sources 176 (2008) 122–127.
[8] X.Z. Fu, J.L. Luo, A.R. Sanger, N. Luo, K.T. Chuang, J. Power Sources 195 (2010) 2659–2663.
[9] X.Z. Fu, J.L. Luo, A.R. Sanger, Z.R. Xu, K.T. Chuang, Electrochim. Acta 55 (2010) 1145–1149.
[10] H. Iwahara, H. Unhida, K. Ono, K. Ogaki, J. Electrochem. Soc. 135 (1988) 529–533.
[11] H. Iwahara, Solid State Ionics 77 (1995) 289–298.
[12] K.H. Ryu, S.M. Haile, Solid State Ionics 125 (1999) 355–367.
[13] T. Shimada, C. Wen, N. Taniguchi, J. Otomo, H. Takahashi, J. Power Sources 131 (2004) 289–292.
[14] C.D. Savaniu, J.C. Vazquez, J.T.S. Irvine, J. Mater. Chem. 15 (2005) 598–604.
[15] C.D. Zuo, S.W. Zha, M.L. Liu, M. Hatano, M. Uchiyama, Adv. Mater. 18 (2006) 3318–3320.
[16] K. Xie, Q.L. Ma, B. Lin, X.Q. Liu, G.Y. Meng, J. Power Sources 170 (2007) 38–41.
[17] L. Yang, C.D. Zuo, S.Z. Wang, Z. Cheng, M.L. Liu, Adv. Mater. 20 (2008) 3280–3283.
[18] E. Fabbri, A. D'Epifanio, E. Di Bartolomeo, S. Licoccia, E. Traversa, Solid State Ionics 179 (2008) 558–564.
[19] S. Barison, M. Battagliarin, T. Cavallin, L. Doubova, M. Fabrizio, C. Mortalo, S. Boldrini, L. Malavasi, R. Gerbasi, J. Mater. Chem. 18 (2008) 5120–5128.
[20] Y. Guo, Y. Lin, R. Ran, Z. Shao, J. Power Sources 193 (2009) 400–407.
[21] Z.T. Tao, L. Bi, Z.W. Zhu, W. Liu, J. Power Sources 194 (2009) 801–804.
[22] H.P. Ding, X.J. Xue, X.Q. Liu, G.Y. Meng, J. Power Sources 195 (2010) 775–778.
[23] X.T. Su, Q.Z. Yan, X.H. Ma, W.F. Zhang, C.C. Ge, Solid State Ionics 177 (2006) 1041–1045.
[24] B.M. Weckhuysen, R.A. Schoonheydt, Catal. Today 51 (1999) 223–232.
[25] Y. Feng, J.L. Luo, K.T. Chuang, J. Phys. Chem. C 112 (2008) 9943–9949.
[26] T. Hibino, A. Hashimoto, M. Suzuki, M. Sano, J. Electrochem. Soc. 149 (2002) A1503–A1508.
[27] B. Liu, M. Terano, J. Mol. Catal. A 172 (2001) 227–240.
[28] A.B. Gaspar, C.A.C. Perez, L.C. Dieguez, Appl. Surf. Sci. 252 (2005) 939–949.